tvst

Retina

Histologic and Immunohistochemical Characterization of GA-Like Pathology in the Rat Subretinal Sodium Iodate Model

Poonam Naik[1], Rhonda Grebe[1], Imran A. Bhutto[1], D. Scott McLeod[1], and Malia M. Edwards[1]

[1] Department of Ophthalmology, Wilmer Eye Institute, Johns Hopkins University School of Medicine, Baltimore, MD, USA

Correspondence: Malia M. Edwards, Wilmer Eye Institute, Johns Hopkins University School of Medicine, Smith Building, Rm M023, 400 North Broadway, Baltimore, MD 21231, USA. e-mail: medwar28@jhmi.edu

Received: September 6, 2023
Accepted: January 2, 2024
Published: February 13, 2024

Keywords: geographic atrophy; phenotypic characterization; RPE; ELM descent; Müller cells rat model; glia

Citation: Naik P, Grebe R, Bhutto IA, McLeod DS, Edwards MM. Histologic and immunohistochemical characterization of GA-like pathology in the rat subretinal sodium iodate model. Transl Vis Sci Technol. 2024;13(2):10, https://doi.org/10.1167/tvst.13.2.10

Purpose: Geographic atrophy (GA) is an advanced form of dry age-related macular degeneration with multifactorial etiology and no well-established treatment. A model recapitulating the hallmarks would serve as a key to understanding the underlying pathologic mechanisms better. In this report, we further characterized our previously reported subretinal sodium iodate model of GA.

Methods: Retinal degeneration was induced in rats (6–8 weeks old) by subretinal injections of $NaIO_3$ as described previously. Animals were sacrificed at 3, 8 and 12 weeks after injection and eyes were fixed or cryopreserved. Some choroids were processed as flatmounts while other eyes were cryopreserved, sectioned, and immunolabeled with a panel of antibodies. Finally, some eyes were prepared for transmission electron microscopic (TEM) analysis.

Results: $NaIO_3$ subretinal injection resulted in a well-defined focal area of retinal pigment epithelium (RPE) degeneration surrounded by viable RPE. These atrophic lesions expanded over time. RPE morphologic changes at the border consisted of hypertrophy, multilayering, and the possible development of a migrating phenotype. Immunostaining of retinal sections demonstrated external limiting membrane descent, outer retinal tubulation (ORT), and extension of Müller cells toward RPE forming a glial membrane in the subretinal space of the atrophic area. TEM findings demonstrated RPE autophagy, cellular constituents of ORT, glial membranes, basal laminar deposits, and defects in Bruch's membrane.

Conclusions: In this study, we showed pathologic features of a rodent model resembling human GA in a temporal order through histology, immunofluorescence, and TEM analysis and gained insights into the cellular and subcellular levels of the GA-like phenotypes.

Translational Relevance: Despite its acute nature, the expansion of atrophy and the GA-like border in this rat model makes it ideal for studying disease progression and provides a treatment window to test potential therapeutics for GA.

Introduction

Age-related macular degeneration (AMD) is the leading cause of vision loss in the elderly in developed countries. There are two major types of AMD: dry, nonneovascular, and wet, neovascular. The most common form, about 80% of cases, is dry AMD. Geographic atrophy (GA), late-stage dry AMD, is a chronic, advanced form of progressive degeneration in the macula. The disease is characterized by sharply demarcated regions of photoreceptors, retinal pigment epithelium (RPE), and choriocapillaris loss.[1] While neovascular AMD can be treated, with varied degrees of success, with intravitreal injections of anti–vascular endothelial growth factor drugs, there are only two drugs recently approved by the US Food and Drug Administration (FDA) for treating GA.

Unfortunately, the complex pathophysiology of GA has not been fully elucidated.[2] Treatments for GA have been hampered because of its multifactorial etiology and lack of an appropriate animal model. Animal models to date mimic some, but not all, aspects of both dry and neovascular AMD. A model that mimics the complex progressive characteristics of GA would provide valuable insights into understanding this disorder. We previously reported an acute injury model in which rats were given subretinal injections of $NaIO_3$.[3] While systemic $NaIO_3$ has been used for decades as a model for RPE loss, this subretinal model has distinct advantages. Systemic injections result in sporadic RPE and photoreceptor loss across the entire retina. By contrast, the subretinal delivery model demonstrates a succinct focal atrophic area. The focal atrophic area is very similar to that seen in human GA. In this model, RPE death is evident at 3 days postinjection, followed by photoreceptor loss at 7 days, concurrent with the development of a glial membrane and choriocapillaris loss by 2 weeks. This model also has a well-demarcated border between atrophic and non-atrophic retina and choroid. As atrophy progresses at the border, the ability to study this specific anatomical region provides a unique opportunity to better understand disease progression.[4]

Here, we further describe the RPE changes within the border region of atrophy and provide evidence for progressive degeneration in the subretinally delivered $NaIO_3$ rat model. We chose 3 weeks as a starting point herein because our focus is atrophic expansion and characterizing the border, as opposed to focusing on the initial cell death induced by $NaIO_3$. With the highly reproducible features of human GA, this model will assist our understanding regarding the pathologic progression and changes at the atrophic border, leading to identification of potential treatment targets.

Materials and Methods

Animals

All animal experiments adhered to the statement of the Association for Research in Vision and Ophthalmology, and the protocols were approved by the animal care and use committee at Johns Hopkins University (Baltimore, MD, USA). Experiments were conducted with adult male (6 to 8 weeks old) Sprague Dawley rats (Envigo, Fredrick, MD, USA). Rats were fed standard laboratory chow (LabDiet; PMI Nutrition International, LLC, Arden Hills, MN, USA) and allowed free access to water with a 12-hour light/12-hour dark cycle in a climate-controlled animal facility.

Subretinal Sodium Iodate Injection

Rats were anesthetized with an intraperitoneal injection of a cocktail containing 100 mg/mL ketamine (VetOne MWI Veterinary Supply Co, Boise, ID, USA) and 20 mg/mL xylazine (Akorn, Inc., Lake Forest, IL, USA). Sodium iodate (S-4007; Sigma-Aldrich, St. Louis, MO, USA) was freshly dissolved in phosphate-buffered saline (PBS) (Quality Biologicals, Gaithersburg, MD, USA) to a concentration of 5 mg/mL. Rats received a single subretinal injection of sterile $NaIO_3$ (1 µL) in each eye as described earlier.[3] As a control, animals were injected with an identical volume of PBS. Animals that received injections of $NaIO_3$ and PBS were euthanized at 3, 8, and 12 weeks. Eyes showing vitreous or subretinal hemorrhage were excluded from the study after observation under a surgical microscope. A minimum of four rats per time point were analyzed using immunohistochemistry (both flatmounts and cyrosections). For transmission electron microscopy (TEM), two rats were analyzed per time point. Despite variability in the initial bleb size between animals, the subretinal injection of $NaIO_3$ consistently induced similar pathological changes in all rats at each time point. Therefore, we chose representative images depicting the pathology at the selected time points.

In Vivo Retinal Imaging Using Spectral-Domain Optical Coherence Tomography

Spectral-domain optical coherence tomography (SD-OCT) was performed on three $NaIO_3$-injected and three PBS-injected rats using the Spectralis imaging system (Heidelberg Engineering, Heidelberg, Germany) specifically designed for small animals. The retina was scanned in nine frames with a total of 17 sections per eye. The automatic real-time (ART) averaging mode allowed for adjustment of the recorded frames to obtain averaged B-scans, which enhanced image quality by reducing movement artifacts and optimizing the signal-to-noise ratio. Subsequent scans were performed on the same rats at 1, 3 and 4 weeks following the subretinal $NaIO_3$ injection, with PBS-injected controls also undergoing imaging. ImageJ (Version 2.14.0/1.54f; National Institutes of Health, Bethesda, MD, USA) was used to measure the expansion.

Flatmount Immunohistochemistry

Eyes were enucleated at 3, 8, and 12 weeks postinjection. One eye from each rat was cryopreserved

while the second eye was processed for choroid/RPE flatmounts. Choroid/RPE tissue was immunostained as described previously.[3] In brief, tissues were fixed overnight in 2% paraformaldehyde (PFA) (Millipore Sigma, Rockville, MD, USA) prepared in Tris-buffered saline (TBS) at 4°C. Subsequently, tissues were washed and blocked using 5% normal goat serum (Jackson Immunoresearch, West Grove, PA, USA) prepared in TBS (Quality Biologicals, Gaithersburg, MD, USA) with 0.1% bovine serum albumin (Sigma Aldrich, Rockville, MD, USA) and 1% Triton X-100 (TBST-BSA) for 6 hours at 4°C. Tissues were then incubated in primary antibody cocktail overnight at 4°C, washed in TBST three times, and incubated in secondary antibody cocktail overnight at 4°C. Prior to imaging, four pie cuts were made to allow the flattening of the choroid/RPE complex. Z stack images at 20× magnification were acquired on a Zeiss LSM 710 confocal microscope (Carl Zeiss Microscopy, LLC, Thornwood, NY, USA) using Zen software. Two-by-two or four-by-four tiled fields with 10% overlap each measuring 2048 × 2048 pixels were captured to visualize the choroid/RPE complex. The imaging settings, including laser power, pinhole, gain, and other capture parameters, were saved and consistently applied to ensure uniform conditions while imaging each choroid/RPE complex. The primary antibodies used were the following: mouse monoclonal RPE-65 antibody (401.8B11.3D9; Novus, Centennial, CO, USA) and rabbit polyclonal zonula occludens 1 (ZO-1) antibody (617300; Invitrogen, Fredrick, MD, USA). Alexa Fluor 647–conjugated and Alexa Fluor Cy3–conjugated secondary antibodies (Invitrogen, Carlsbad, CA, USA) were used for detection of primary antibodies.

Immunohistochemistry on Cryosections

Immunohistochemistry was performed as described previously.[3] In brief, cryosections of the eye were permeabilized with cold methanol, air dried, and then washed in TBS before incubating in primary antibody cocktail for 2 hours at room temperature (RT) followed by a cocktail of secondary antibodies for 30 minutes at RT. The following primary antibodies were used: chicken anti–glial fibrillary acidic protein antibody (AB5541; Millipore, Burlington, MA, USA), mouse rhodopsin monoclonal antibody (MBS803218; MyBioSource, San Diego, CA, USA), and rabbit ionized calcium binding adaptor molecule 1 (Iba1) (019-19741; WAKO, Osaka, Japan). Alexa Fluor 647–conjugated and Alexa Fluor Cy3–conjugated secondary antibodies (Invitrogen) were used for detection of primary antibodies. Sections were counter-stained with 4′,6-diamidino-2-phenylindole (DAPI). Slides were coverslipped using Dako cytomation mounting media (Agilent, Santa Clara, CA, USA). Images were acquired on a Zeiss 710 confocal microscope.

Transmission Electron Microscopy

For TEM, eyes were cut to include the border region and were processed as described previously.[5] Briefly, full-thickness eyewall pieces were fixed in a mixture of 2.5% glutaraldehyde and 2% paraformaldehyde (EMS, Hatfield, PA, USA) in 1 M cacodylate buffer (Millipore Sigma) at pH 7.3 for at least 24 hours at 4°C. One-micron semi-thin sections for light microscopy were cut on a Sorvall MT ultramicrotome and stained with a filtered solution containing 1% toluidine blue O (Millipore Sigma) and 1% sodium borate (Electron Microscopy Sciences, Hatfield, PA, USA). Areas for TEM were selected and trimmed for ultramicrotomy. Ultra-thin sections (68–72 nm) were cut on a Leica EM UC7 ultramicrotome (Leica Microsystems, Vienna, Austria) using a 3.5-mm Diatome diamond knife, transferred to 3.5-mm thin bar copper grids, and stained for 10 minutes with 2% aqueous uranyl acetate and 3 minutes with lead citrate (Electron Microscopy Sciences). Images were acquired with a Hitachi H7600 (Tokyo, Japan) transmission electron microscope at 80 kV. For ultrastructural comparison in TEM, the non-pathological area of the same eye was considered as control.

Results

Expansion of the Atrophy Following Subretinal $NaIO_3$ Injection

PBS-injected rats had a normal OCT with normal thickness in all retinal layers and intact RPE monolayer at 1 week (Fig. 1A). These eyes remained normal throughout all time points. As shown in our previous report, distinct areas contained RPE loss as well as outer nuclear layer (ONL) thinning in all $NaIO_3$-injected rats at 1 week (Fig. 1B). It was difficult to align the exact area at multiple time points, and in most eyes, only one border was visible. Therefore, it was not possible to measure the size of the lesion accurately over time in all rats. In one rat, we observed a blood vessel outside the atrophic area, which we utilized to measure expansion. To quantify the linear expansion of atrophy, we measured the distance from the atrophic border to this large retinal blood vessel in the inner retina (arrowheads) at the 1-week (Fig. 1B), 3-weeks (Fig. 1C), and

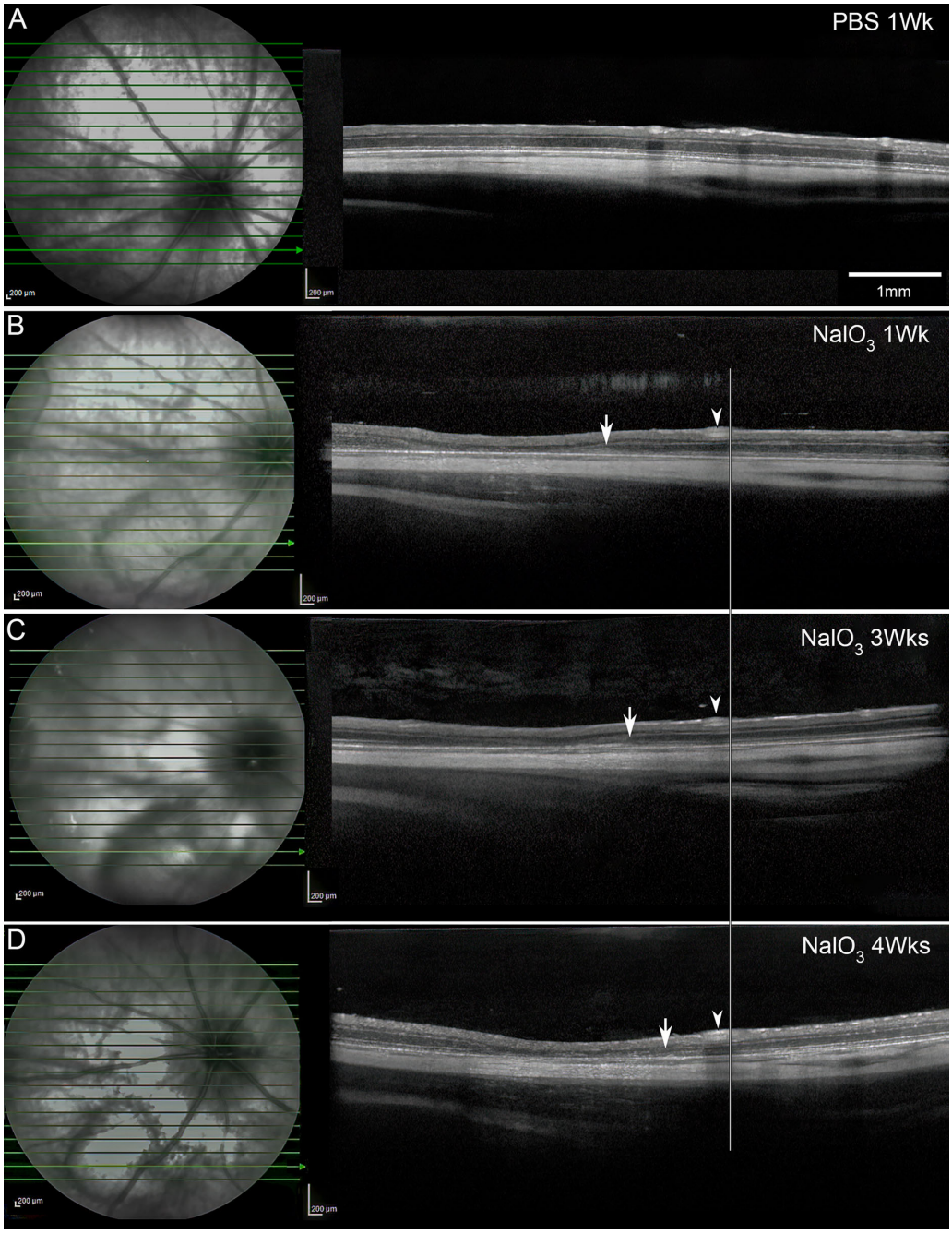

Figure 1. En face OCT images with respective B-scans of a PBS-injected control eye shows the normal retinal and RPE appearance (**A**). The injected area is not visible. En face OCT images with respective B-scans of a $NaIO_3$-injected eye at 1 week (**B**), 3 weeks (**C**), and 4 weeks (**D**) postinjection. *Green line* represents location of cross-sectional B-scan on initial en face OCT. B-scans enable delineation of the various retinal layers, including the hyperreflective outer retinal bands. The inner retinal blood vessel (indicated by the *arrowheads*), considered a common landmark in the scans, has aligned the outer vessel wall with a line for the measurement to the atrophic border in each scan (*arrows*). The distance from the retinal vessel to the edge of atrophy was measured, revealing an expansion of 0.256 mm and 0.7 mm between 1 and 3 weeks and 1 and 4 weeks, respectively. *Scale bar* in **A**: 1 mm for all.

4-weeks scans (Fig. 1D). The distance was measured to the edge of atrophy (arrows), which was evident by consequent loss of the ONL. In the 1-week scan, the distance was 1.34 mm (Fig. 1A), compared to 1.09 mm in the 3-weeks scan (Fig. 1B) and 0.7 mm at 4 weeks (Fig. 1C). Therefore, the area of atrophy expanded by a distance of 0.256 mm from 1 to 3 weeks and by 0.6 mm from 1 to 4 weeks.

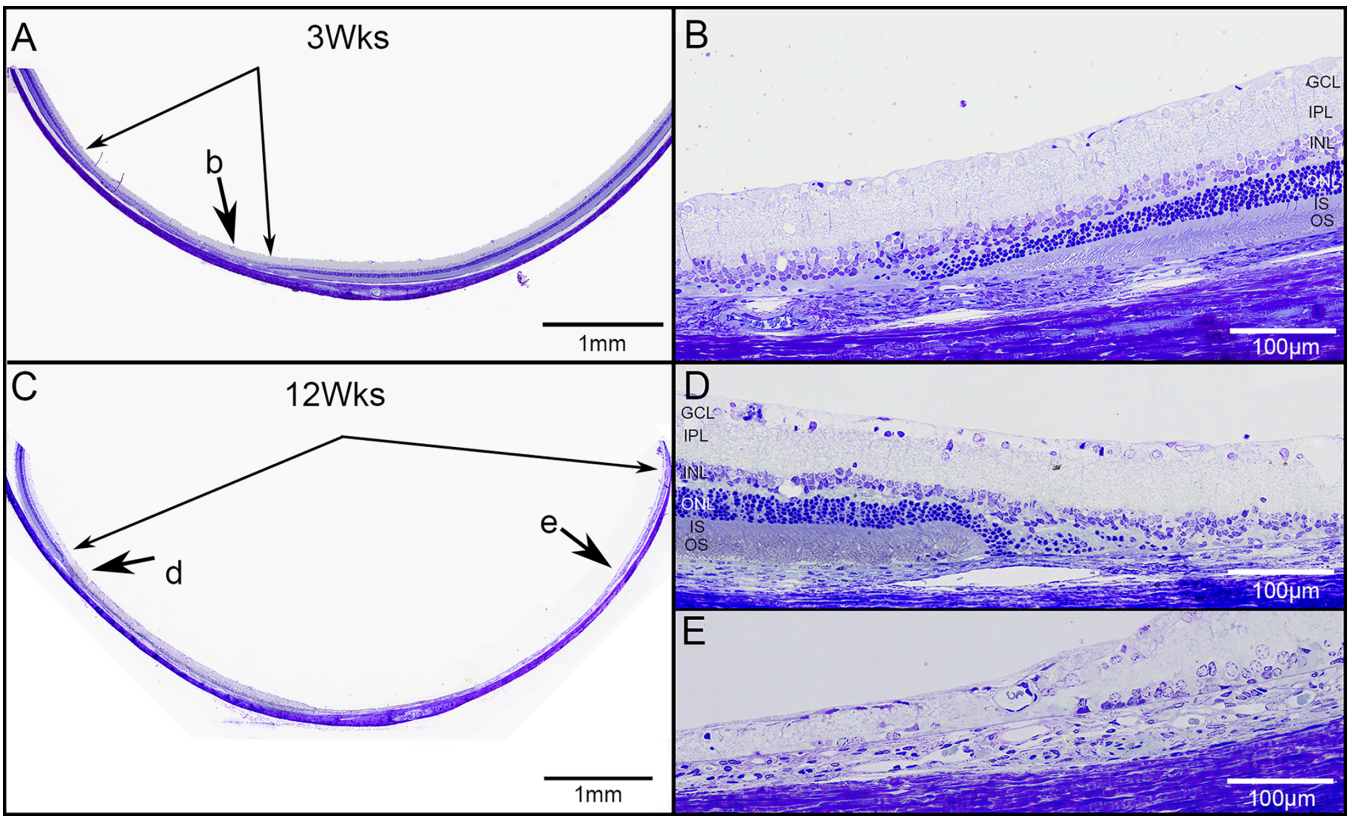

Figure 2. Representative toluidine blue–stained semi-thin sections at low and high magnification from 3 weeks (**A**, **B**) and 12 weeks (**C**–**E**) post-$NaIO_3$ injection. The atrophic area (*paired arrows* in **A**) at 3 weeks postinjection demonstrates that the loss of the RPE is sharply delimited by the ELM descent (**A**). A magnified view of the region indicated by arrow "b" in **A** shows the border of atrophy (**B**). The inner nuclear, inner plexiform, ganglion cell, and nerve fiber layers are all intact at 3 weeks in the atrophic region. In the case of the 12 weeks post-$NaIO_3$ injection eyes, the atrophic area had greatly expanded (*paired arrows* in **C**). Higher-magnification views of the region indicated by arrow "d" and "e" in **C** shows the ELM descents on each side of the atrophic border. The atrophic side of ELM descent shows the downward slope of the ONL as well as gradual thinning of the INL while the inner plexiform, nerve fiber, and ganglion cell layers are intact (**D**). A more severely affected area of atrophy at 12 weeks is observed (**E**) where most of retinal layers are degenerated. *Scale bars*: 1 mm for **A**, **C**; 100 µm for **B**, **D**, **E**.

Toluidine blue–stained semi-thin sections showed well-demarcated atrophic borders 3 weeks after $NaIO_3$ injection (Fig. 2A). The atrophic area was delimited by the external limiting membrane (ELM) descent with concomitant loss of ONL, photoreceptor inner segments (ISs), and outer segments (OSs) and absence of the RPE (Fig. 2B). ELM descent is a curved line that delineates the atrophic border signified by OS absence and IS shortening at the descent. The atrophic region was bounded by a histologically normal retina. The atrophic area contained prominent borders on each side even at 12 weeks postinjection (Fig. 2C). Similar to 3 weeks, we observed gradual thinning of the ONL, IS/OS, and complete RPE loss demarcated by the ELM descent (Fig. 2D). The ONL exhibited a gradual increase in thickness away from the border, and photoreceptor inner and outer segments also became evident (Fig. 2D). Twelve weeks after $NaIO_3$ injection, we observed a severely atrophic area of retina, the presumed initial injection site, and an area with considerably less retinal thinning, which we have termed the transition zone. The initial injected area had a severely attenuated inner nuclear layer (INL) and complete loss of the photoreceptors and RPE (Fig. 2E).

Immunofluorescence and Ultrastructural Analysis of Morphologic Alterations in RPE

Choroid/RPE flatmounts were immunolabeled with RPE-65 antibody to evaluate the sequential changes at 3, 8, and 12 weeks after $NaIO_3$ injection (Fig. 3). The PBS-injected eyes showed a relatively uniform RPE-65 labeling (Fig. 3A). The atrophic border regions of $NaIO_3$-injected eyes were well defined and exhibited abnormal RPE cells while the RPE monolayer

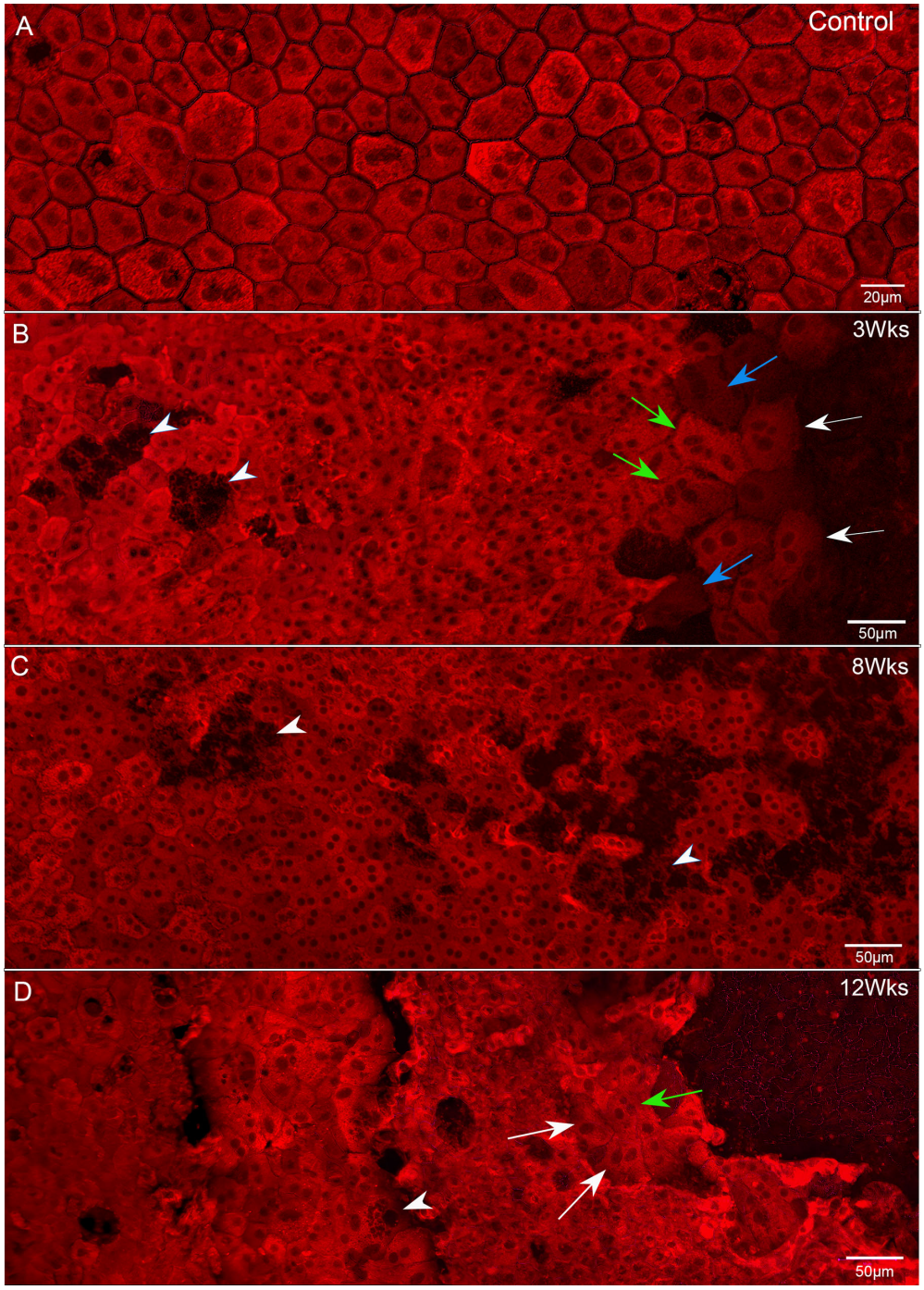

Figure 3. Confocal images of choroid/RPE flatmounts from a control (**A**) and $NaIO_3$-injected rats (**B–D**) immunolabeled with RPE-65 (*red*). The control demonstrates a monolayer of RPE cells with cobblestone morphology (**A**). In the 3 weeks $NaIO_3$-injected rat, hypertrophic (*white arrows*), fusiform (*blue arrows*), and multinucleated RPE (*green arrows*) are apparent at the border. Areas exhibiting loss of RPE-65 were observed away from the atrophic border (*arrowheads*). RPE-65 staining at 8 weeks postinjection shows considerable morphologic heterogeneity in shape and size with progressive degeneration away from the atrophy (**C**). Few areas show punctate RPE-65 staining (*arrowheads*) (**C**). The border region at 12 weeks post-$NaIO_3$ injection exhibits hypertrophic (*white arrows*), multinucleated RPE (*green arrow*), and punctate RPE-65 staining (*arrowhead*). *Scale bars*: 20 μm for **A**, 50 μm for **B–D**.

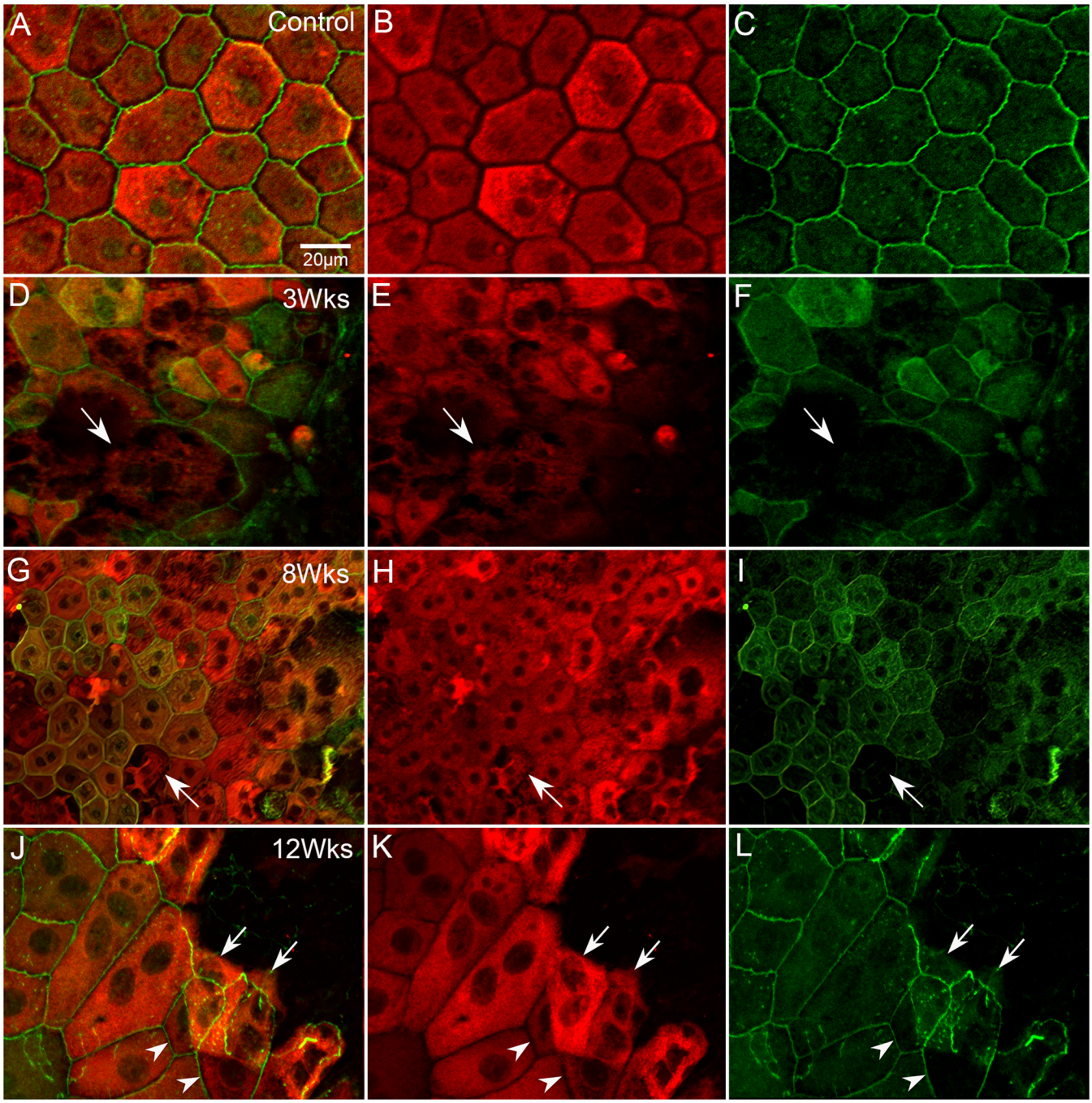

Figure 4. Confocal images of choroid/RPE flatmounts from a control rat (**A–C**) and $NaIO_3$-injected rats 3 weeks (**D–F**), 8 weeks (**G–I**), and 12 weeks (**J–L**) postinjection immunolabeled with RPE-65 (*red*) and ZO-1 (*green*). The control rat is characterized by a monolayer of hexagonally shaped RPE cells with fairly uniform RPE-65 staining (**A**, **B**) and ZO-1 staining at the cell–cell junctions (**C**). In the $NaIO_3$-injected eyes, a stacked Z-series confocal image shows RPE-65 staining alterations (**E**, **H**, **K**) and ZO-1 junctional alterations (**F**, **I**, **L**) at the atrophic border. Anteriorly migrated RPE cells with atypical RPE-65 staining (*arrow* in **D–F**) and a second layer of RPE cells underlying the superficial cells with lost ZO-1 staining (*arrowheads* in **L**). The junctional complexes at the border are discontinuous, fragmented, and thinned as demonstrated with ZO-1 immunolabeling (**L**). *Scale bar*: 20 μm for **A–F**.

was completely lost in the atrophic zone (Fig. 3B). Notably, the RPE cells at the border were hypertrophic (white arrows) and fusiform (blue arrows) in appearance and multinucleated (green arrows). Few areas with complete RPE-65 loss were observed away from the atrophic border (arrowheads). At 8 weeks post-$NaIO_3$ injection, the shape and size of RPE cells appeared highly variable compared to the control

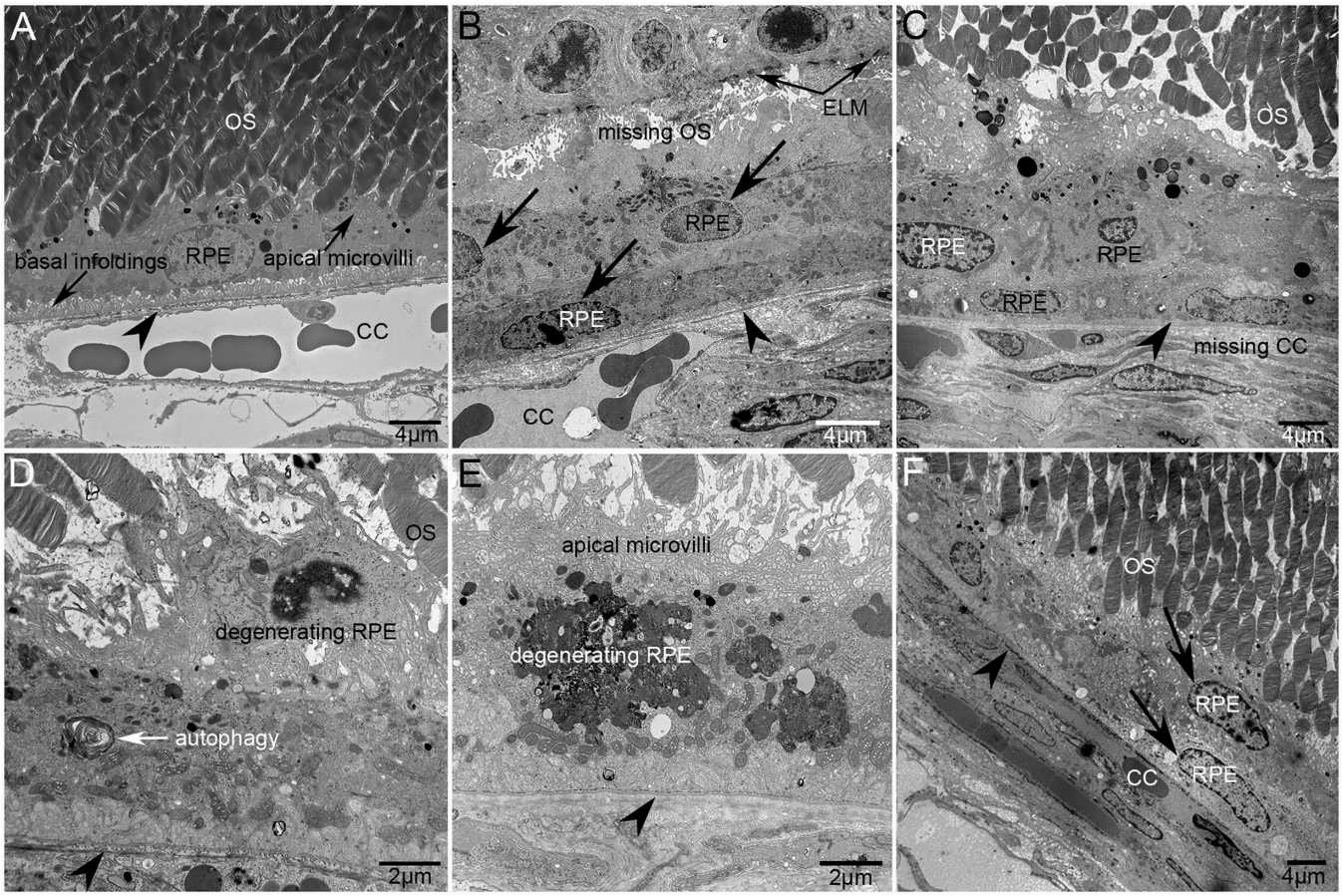

Figure 5. Representative electron micrograph of Bruch's membrane/RPE/photoreceptor complex in a control eye (**A**) shows the normal morphology of RPE cells with long and dense apical processes and prominent basal infoldings. The apical microvilli (*up-facing arrow*) ensheath the orderly array of the normal photoreceptor outer segments while RPE basal infoldings (*downward-facing arrow*) are adjacent to a deposit-free BrM (**A**). RPE cells (*arrows*) in a 3 weeks post-$NaIO_3$ injection rat with disorganized and shorter microvilli form multiple layers in the atrophic aspect of the border region (**B**). *Paired arrows* indicate the ELM. A double layer of RPE was observed at 8 weeks post-$NaIO_3$ injection near the atrophic border (**C**). Degenerating RPE cells with nuclear changes and disorganized OSs were also observed (**D**, **E**). Degenerating RPE and autophagy within the RPE (*white arrow* in **D**) were observed near the border at 8 weeks (**D**, **E**). At 12 weeks, RPE cells (*arrows*) in the nonatrophic aspect of the border region show multilayering (**F**) and viable OSs are observed. *Arrowheads* in all panels indicate BrM. *Scale bars*: 4 μm for **A–C**, 2 μm for **D–E**, 4 μm for **F**.

(Fig. 3C). Similar to the observation at 3 weeks, the cells appeared either flattened or with a fusiform morphology at the border area (not shown). In the case of 12 weeks, we noted RPE hypertrophy at the border (white arrows) as well as punctate RPE-65 staining (arrowhead) and multinucleated (greater than 2 nuclei/cell) RPE cells (green arrow) (Fig. 3D). We further stained the choroid/RPE complex in the controls and at 3, 8, and 12 weeks with ZO-1. In the control, each RPE cell was delimited by well-defined junctional complexes with uniform ZO-1 (Figs. 4A, 4C) and RPE-65 staining (Figs. 4A, 4B). At both 3 and 8 weeks, RPE cells exhibited diminished RPE-65 expression and aberrant ZO-1 expression (arrows), particularly near the border (Figs. 4D, 4G). Notably, at 12 weeks, multilayered RPE cells were apparent at the atrophic border (Fig. 4J). The redundant RPE at 12 weeks demonstrated RPE-65 staining (arrows) intensity, which was similar to controls (Fig. 4K). RPE cells that appeared to have migrated anteriorly toward the atrophic border did not exhibit ZO-1 staining (arrowheads) at their leading edge while the cells beneath demonstrated interruptions in ZO-1–positive junctions (Fig. 4L).

TEM analysis of the PBS-injected control eyes demonstrated normal photoreceptor OSs, a uniform RPE monolayer with prominent basal infoldings and long apical process, an intact deposit free Bruch's membrane (BrM) and viable choriocapillaris (Fig. 5A). Three weeks following $NaIO_3$ injection, the areas of multilayered RPE cells near the border region had shortened and reduced density

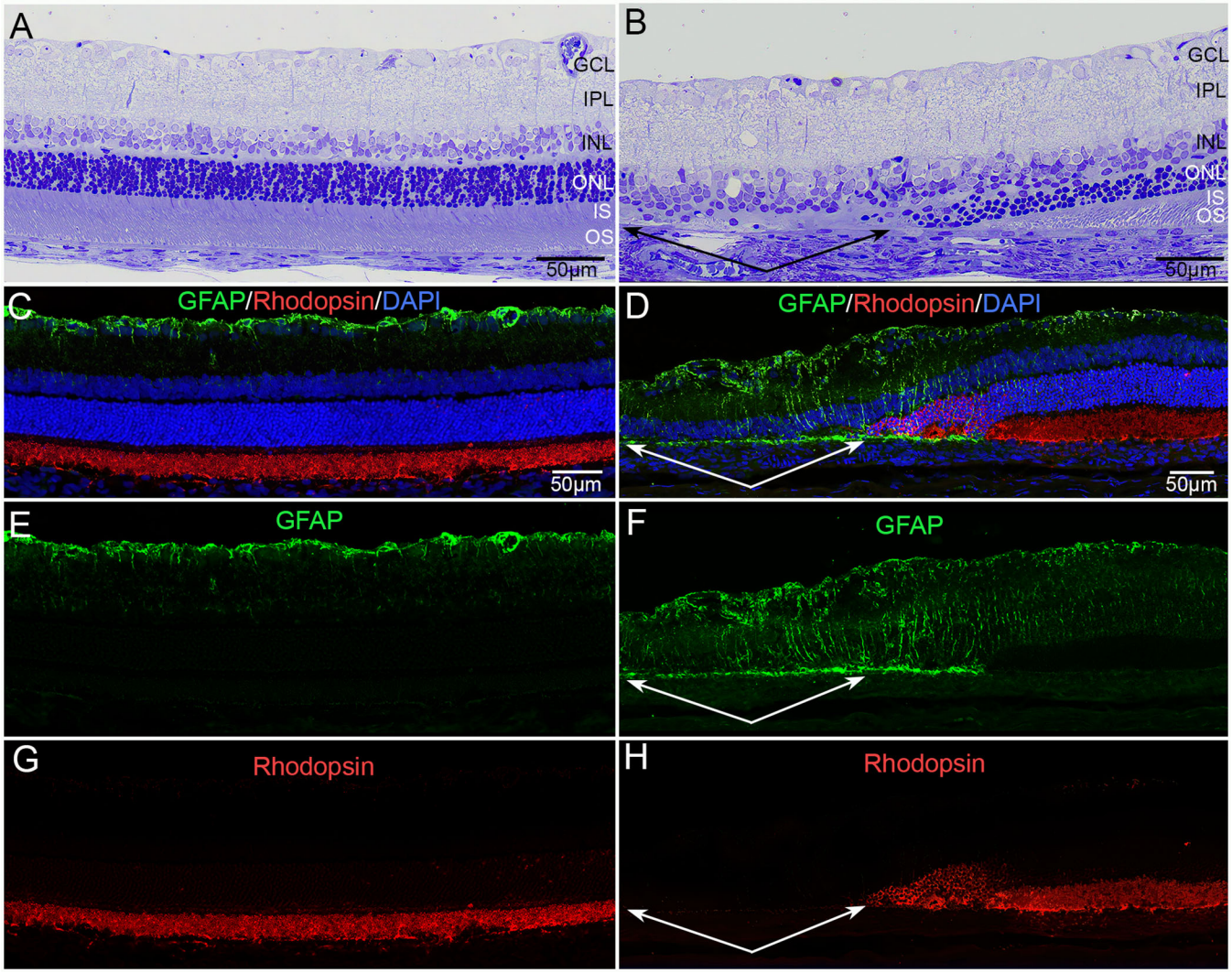

Figure 6. Representative semi-thin toluidine blue–stained sections from a 3-week $NaIO_3$-injected eye in the nonatrophic region (**A**) and at the atrophic border (**B**). The ELM descent of the atrophic border is shown in **B** and demonstrates a gradual shortening of the photoreceptor inner/outer segments, decreasing rows of photoreceptor nuclei and complete RPE degeneration in the atrophic region (*paired arrows*). In immunohistochemical stained cryosections from the nonatrophic regions of 3-week postinjected eyes, glial fibrillary acidic protein (GFAP) immunoreactivity was limited to astrocytes of the nerve fiber/ganglion cell layers (**C**, **E**) and rhodopsin immunostaining was confined to rod OS (**C**, **G**). At the border of atrophy, activated Müller cells spanning the entire retinal thickness expressed GFAP (**D**, **F**), as did a glial membrane, which occupied the subretinal space of the atrophic area (*paired arrows* in **D**, **F**). This glial membrane extended into the region of the ELM descent at the border. At the atrophic aspect of the ELM descent, rhodopsin was mislocalized to the perinuclear region of surviving photoreceptor cells that were devoid of inner/outer segments. *Scale bars*: 50 µm for **A**–**H**.

of apical microvilli (Fig. 5B). The basal infoldings were also less prominent, and there were no photoreceptor OSs. Eight weeks following $NaIO_3$ injection, RPE multilayering was observed at the border where OSs were disorganized and loosely in contact with the RPE apical processes (Fig. 5C). In addition, we observed degenerating RPE cells at the border (Figs. 5D, 5E). Similarly at 12 weeks after $NaIO_3$ injection, RPE multilayering was observed adjacent to border area on the nonatrophic side (Fig. 5F).

Atrophic Border Defined by External Limiting Membrane Descent

Toluidine blue–stained semi-thin sections of eyes from 3 weeks post-$NaIO_3$ injection demonstrated a typical retinal architecture with a normal arrangement of layers from the inner limiting membrane (ILM) to the photoreceptor OSs in the nonatrophic regions (Fig. 6A). The RPE monolayer was intact, photoreceptor OS/IS were unremarkable, the ONL thickness varied from 8 to 10 nuclei, and the INL was four to

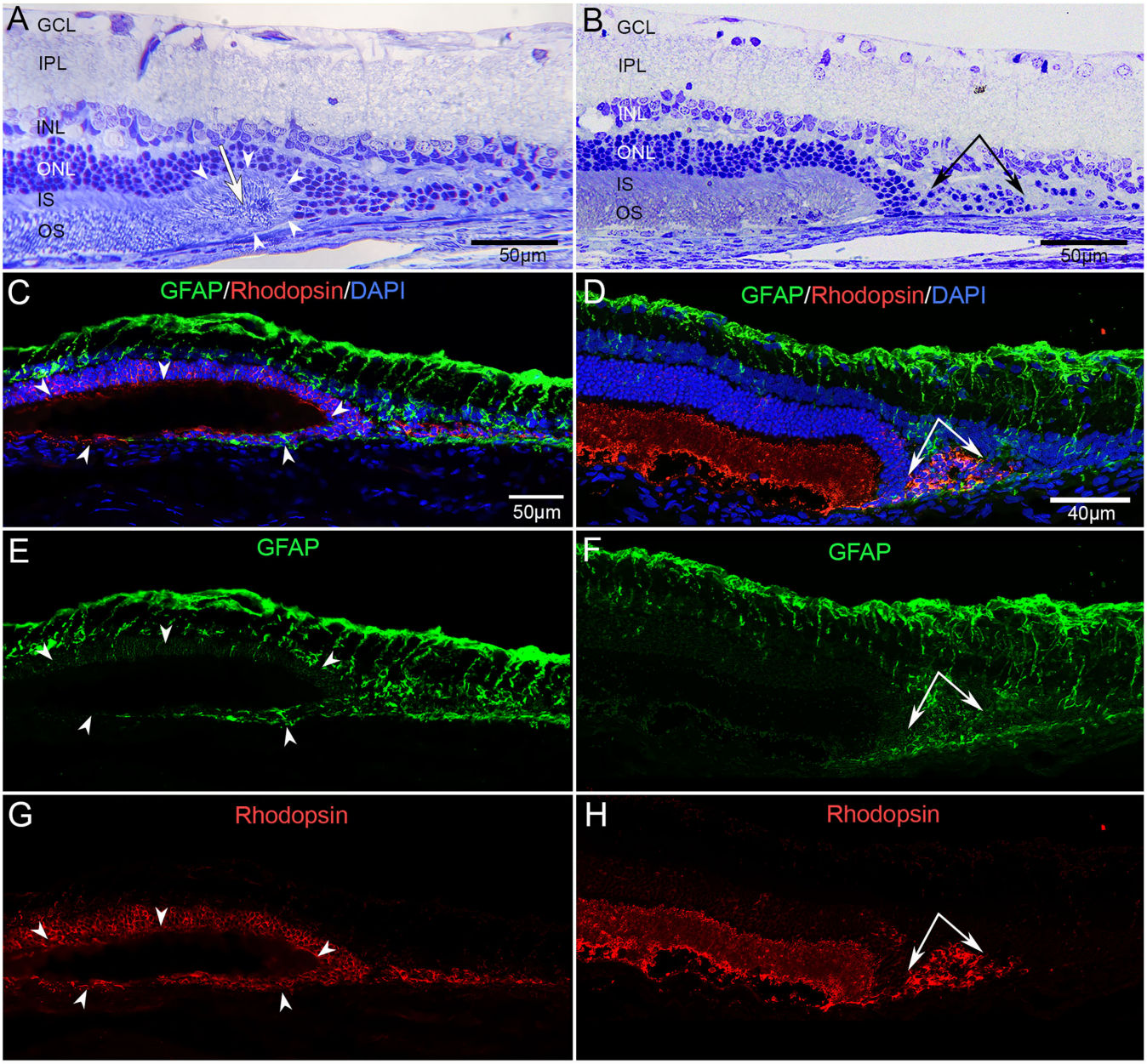

Figure 7. Toluidine blue–stained semi-thin sections of $NaIO_3$-injected eyes at 8 weeks (**A**) and 12 weeks (**B**) showing the ELM descent at the atrophic border. The descent at these time points shows a more curved shape than at 3 weeks postinjection. Some sections showed apparent ORTs, which consisted of degenerating photoreceptors arranged in a circular or tubular fashion (*arrow* in **A**) bordered by the scrolled ELM (*arrowheads* in **A**). Surviving photoreceptor nuclei were seen in the atrophic aspect of the ELM descent at 12 weeks (*paired arrows* in **B**). Confocal images of $NaIO_3$-injected eyes showing the ELM descent region at 8 weeks (**C**) and 12 weeks (**D**) immunolabeled with GFAP and rhodopsin and counterstained with DAPI. Just adjacent to the nonatrophic aspect of the ELM descent in an 8-week eye, an ORT shows increased GFAP staining of Müller cell processes (**E**) and rhodopsin localized to the OS within the ORT (**G**). Internal to the ORT, rhodopsin was mislocalized to the perinuclear region of photoreceptor cells. At 12 weeks, GFAP-positive cell processes in the atrophic aspect of the ELM descent were observed throughout the degenerating retina and in a subretinal glial membrane (**F**). Aggregates of rod nuclei devoid of IS/OS at the atrophic border (*paired arrows* in **D**, **F**, **H**) demonstrate strong perinuclear rhodopsin immunoreactivity (**D**, **H**). *Scale bars*: 50 µm for **A**, **B**; 25 µm for **C**, **E**, **G**; 40 µm for **D**, **F**, **H**.

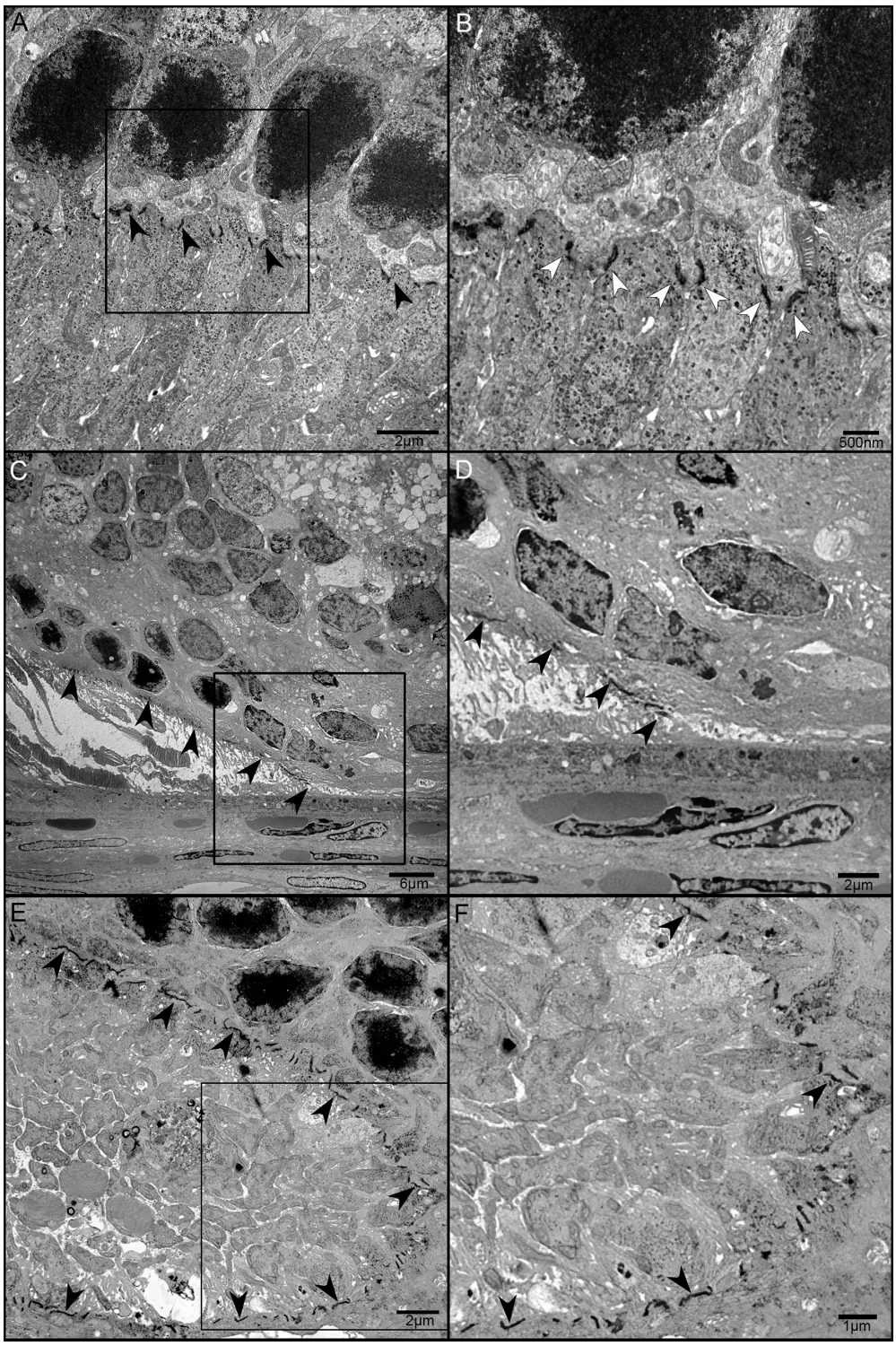

Figure 8. TEM images showing normal ELM structure in the nonatrophic region from a 12 weeks $NaIO_3$-injected rat at low (**A**) and higher magnification (**B**). The ELM consists of comma-shaped junctional complexes between the photoreceptor inner segments and Müller cell processes (*arrowheads*). In the border region of 12 weeks $NaIO_3$-injected rats, the ELM descended toward BrM, where junctional complexes (*arrowheads*) had a more linear appearance until they disappeared in regions of complete atrophy (**C**, **D**). ORT in another 12 weeks $NaIO_3$-injected rat was demarcated by the convolution of the disrupted ELM (*arrowheads*) around the degenerating photoreceptor inner and outer segments, which are retracted inwardly (**E**, **F**). Boxed regions in **A**, **C**, and **E** are shown at higher magnification in **B**, **D**, and **F**. *Scale bars*: 2 µm for **A**, **E**; 500 nm for **B**; 6 µm for **C**; 1 µm for **D**, **F**.

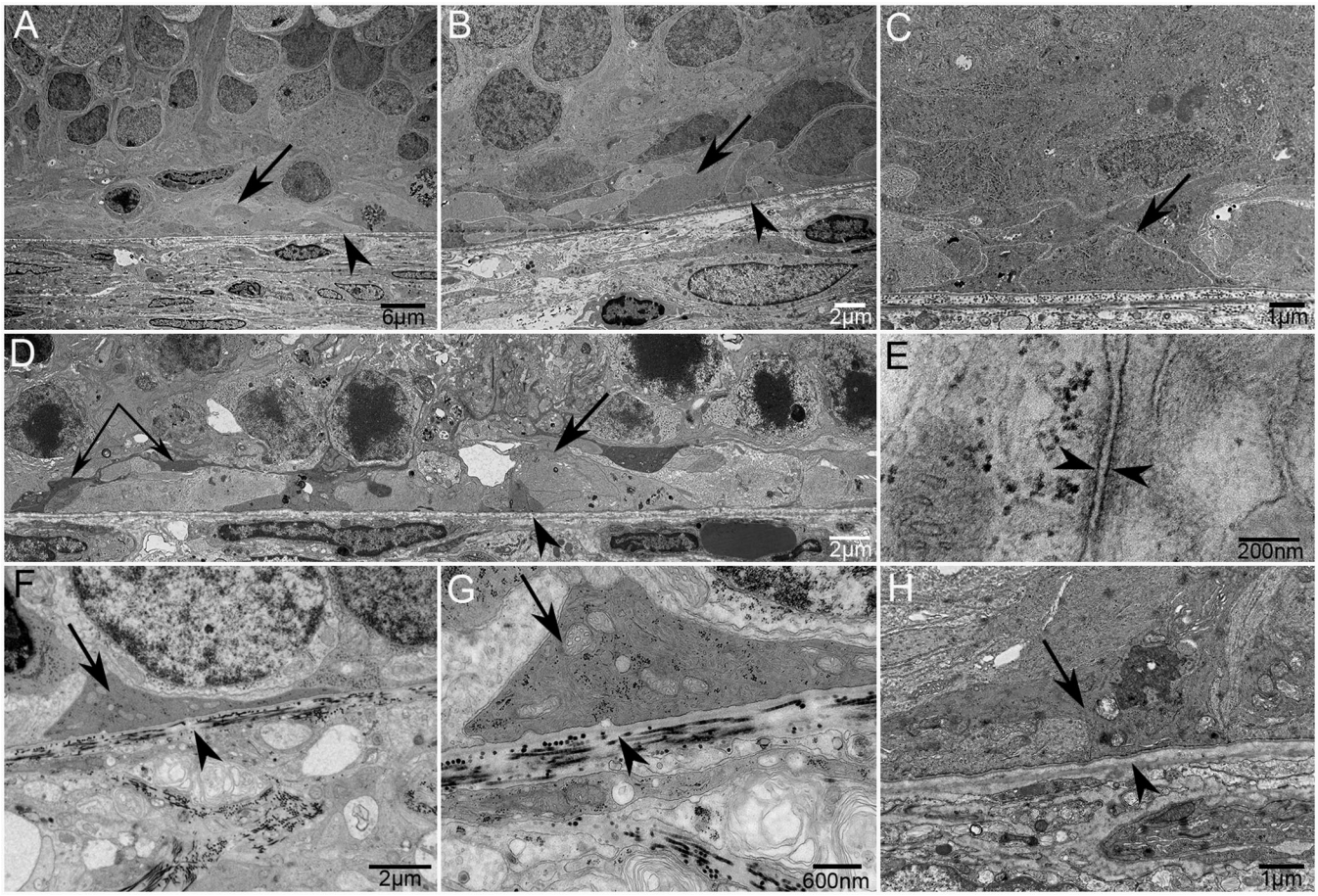

Figure 9. TEM images showing subretinal location of glial cell processes in $NaIO_3$-injected rats at 3 weeks, 8 weeks, and 12 weeks postinjection. Müller cell processes (*arrows*) occupy the subretinal space above BrM (*arrowhead*) in the atrophic region at 3 weeks where the RPE cells and photoreceptors have degenerated (**A**, **B**). Glial cell processes extend along BrM in the subretinal region (*arrows*) where photoreceptors and RPE cells have atrophied at both 3 weeks (**C**) and 8 weeks (**D**) in $NaIO_3$-injected rats. Müller cell processes are indicated by the *paired arrows* in 8-week $NaIO_3$-injected rats (**D**). *Opposing arrowheads* indicate intracellular junctions in the glial membrane observed in 8-week postinjection rats (**E**). Lower (**F**) and higher (**G**) magnification revealed Müller cell endfeet-like processes (*arrows*) above BrM (*arrowheads*) at 12 weeks. Electron-dense glial processes were observed extending along BrM in the subretinal region in the atrophic area at 12 weeks postinjection (**H**). *Scale bars*: 6 µm for **A**; 2 µm for **B**, **D**, **F**; 1 µm for **C**, **H**; 200 nm for **E**; and 600 nm for **G**.

five nuclei thick. By contrast, in the atrophic border regions (Fig. 6B), there was a concomitant degeneration of RPE and photoreceptor cells. The ONL tapered from 8 to 10 nuclei thick in nonatrophic regions to one to two layers at the border and was absent in regions of total atrophy. The INL was three to four nuclei thick at the border. The inner and outer segments gradually became shorter and disappeared completely at the edge of atrophy (Fig. 6B). The ELM descent adjacent to the atrophic region assumed an oblique shape.

In cryosections from PBS-injected control rats immunolabeled with glial fibrillary acidic protein (GFAP) and rhodopsin, GFAP immunostaining was found primarily restricted to astrocytes in the nerve fiber layer and ganglion cell layer (GCL) (Figs. 6C, 6E). Müller cell processes spanning other retinal layers were unlabeled or had extremely weak GFAP expression. In the control retinas, rhodopsin immunoreactivity showed uniform staining of rod outer segments (Figs. 6C, 6G). In the 3-week postinjection eyes, we observed increased expression of GFAP by Müller cells (Figs. 6D, 6F) in the atrophic and border regions. GFAP-positive Müller cell processes spanned the entire retina in the atrophic region and extended into the subretinal space (Fig. 6F). Within these atrophic regions, there was no rhodopsin expression, which was consistent with complete photoreceptor cell loss (Fig. 6H). Moreover, at the border region adjacent to the ELM descent, there were aggregates of photoreceptor nuclei that expressed intense perinuclear rhodopsin in the absence of inner/outer segments. The ELM descent assumed an oblique shape at 3 weeks.

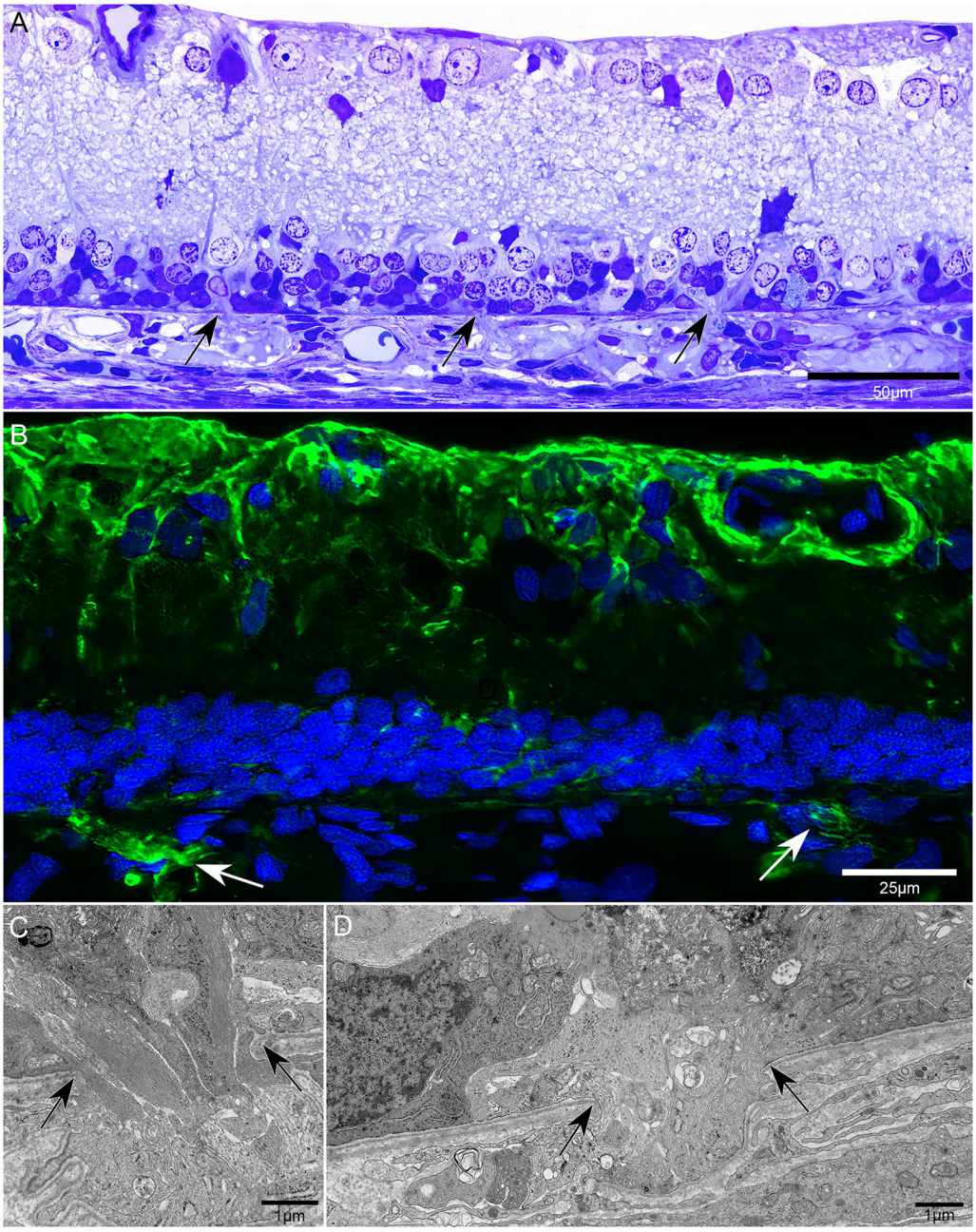

Figure 10. Semi-thin section stained with toluidine blue at 12 weeks postinjection showing glial cell processes invading the choroidal stroma through defects in Bruch's membrane at three separate locations in the atrophic region (**A**). GFAP immunoreactive processes of Müller cells of the atrophic retina (*arrows*) extending into the choroidal stroma (**B**). TEM images showing electron-dense (**C**) and less dense processes (**D**) extending through breaks in BrM (*arrows*). *Scale bars*: 50 µm for **A**, 25 µm for **B**, and 1 µm for **C**, **D**.

In 8- and 12-week post-$NaIO_3$ injection eyes (Figs. 7A, 7B), toluidine blue–stained semi-thin sections demonstrated an ELM descent at the atrophic borders as has been described in human GA. On the non-atrophic aspect of the curved ELM descent, photoreceptors shifted their orientations from orthogonal to parallel towards BrM (Fig. 7A). The ELM descended towards BrM and the adjacent photoreceptors were scrolled into an outer retinal tubular structure (Fig. 7A). Photoreceptor nuclei devoid of inner and outer segments were observed just anterior to the edge of the ELM descent (Figs. 7A, 7B). The ONL decreased from approximately eight to three nuclei thick in this region. We also observed increased Müller cell GFAP immunoreactivity in the border and atrophic regions at 8 and 12 weeks postinjection

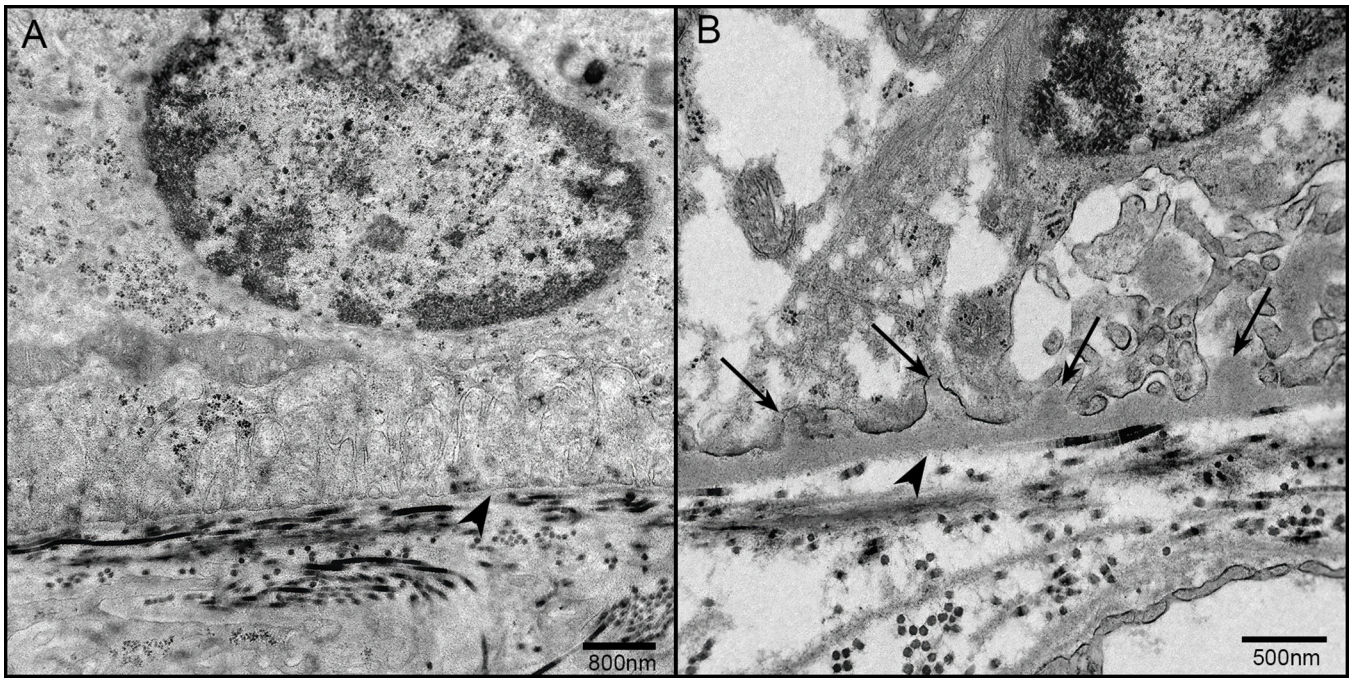

Figure 11. TEM images showing BrM (*arrowhead*) and RPE basal infoldings in a nonatrophic region of $NaIO_3$-injected rat (**A**). Sub-RPE basal laminar deposits (*arrows*), with a scalloped appearance, were observed interposed between the basement membrane and basal lamina of RPE in a 12 weeks postinjection rat (**B**). BrM is indicated by *arrowheads*. *Scale bars*: 800 nm for **A**, 500 nm for **B**.

(Figs. 7C–F). GFAP-positive Müller cell processes lost their radial orientation, and their processes adopted a more horizontal or parallel morphology. They formed membranes in the subretinal space. Again, the atrophic areas in 8- and 12-week post-$NaIO_3$ injected eyes demonstrated photoreceptor degeneration, which was reflected by the lack of rhodopsin immunoreactivity (Figs. 7G, 7H). An exception to this were aggregates of nuclei located closely to the atrophic aspect of the ELM descent. These cells had a nuclear morphology similar to rods, were devoid of inner/outer segments, and yet strongly expressed perinuclear rhodopsin (Fig. 7H). We also observed mislocalized rhodopsin immunostaining in the ONL on the nonatrophic aspect of the ELM descent where inner/outer segments were still intact. Additionally, rhodopsin immunostaining was observed in the ONL opposed to sites where an apparent outer retinal tubulation (ORT) was present (Fig. 7G).

In the nonatrophic regions, TEM revealed the ELM as regularly spaced comma-shaped junctions between Müller cells and photoreceptor inner segments (Figs. 8A, 8B). At the atrophic edge in 12-week post-$NaIO_3$ injection eyes, the ELM at the descent was irregularly spaced and more linear in appearance (Figs. 8C, 8D). Only fragmented debris from photoreceptor inner/outer segments was present at this site. ORTs in the nonatrophic aspect of the border region demonstrated photoreceptor inner segments surrounded by an ELM represented by the electron-dense junctions between Müller cells and degenerating inner segments (Figs. 8E, 8F).

Ultrastructural Analysis of the Retinochoroidal Interface

TEM demonstrated that glial cell processes had invaded the subretinal space in the atrophic regions of $NaIO_3$-injected eyes. Multilayered glial membranes with different electron density were evident. Cell processes with either dense or less dense filaments were identified at 3 weeks (Figs. 9A–C) and 8 weeks postinjection (Fig. 9D). Electron-dense glial cell processes within the membranes were Müller cells based on their ultrastructural characteristics. Intracellular junctions were observed in the glial membrane (Fig. 9E). In some areas, Müller cells created endfeet-like processes, as normally seen at the ILM, on BrM (Figs. 9F, 9G). Müller cell processes extended horizontally across the outer retinal/BrM interface (Fig. 9H). At 12 weeks post-$NaIO_3$ injection, semithin toluidine blue–stained sections showed Müller cell processes breaching defects in BrM and extending into the choroidal stroma with some enveloping or invading degenerative choriocapillaris lumen (Fig. 10A). We further observed that these cell

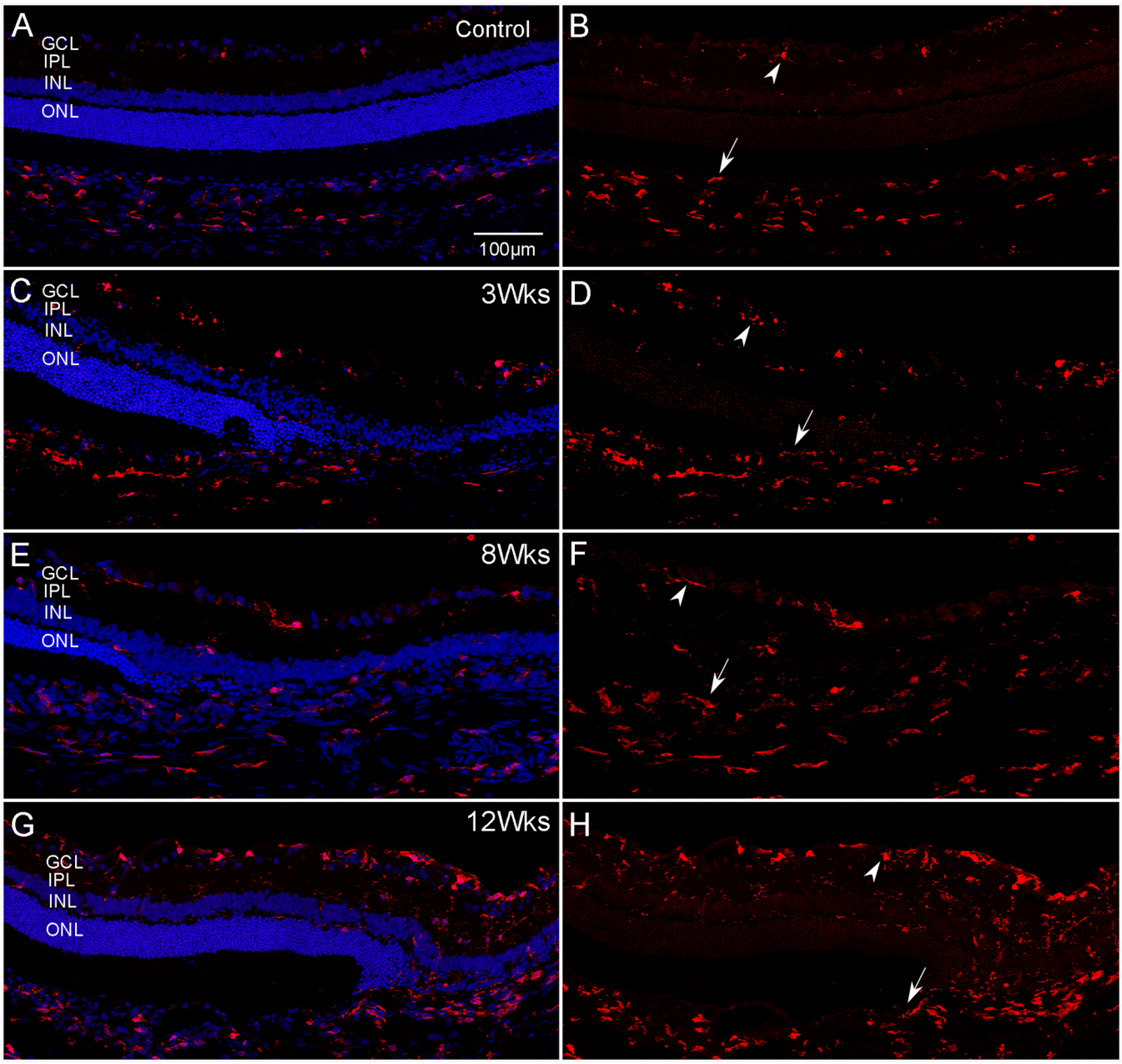

Figure 12. Representative sections from a control rat (**A**, **B**) and 3 weeks (**C**, **D**), 8 weeks (**E**, **F**), and 12 weeks (**G**, **H**) post-$NaIO_3$ injection immunolabeled with Iba-1 (*red*) and counterstained with DAPI (*blue*). In the control rat, $Iba1^+$ microglia/macrophages were observed in the GCL and the INL layers of the retina (*arrowhead* in **B**) and in the choroidal stroma (*arrow* in **B**). Compared to the control, post-$NaIO_3$-injected eyes at 3 weeks (**D**), 8 weeks (**F**), and 12 weeks (**H**) all showed a prominent increase in the $Iba1^+$ cells in retina and choroid. *Scale bar*: 100 μm.

processes were $GFAP^+$, indicating that they were likely activated Müller cells (Fig. 10B). TEM clearly showed electron-dense Müller cell processes extending through defects in BrM into the choroidal stroma (Fig. 10C). Similarly, we observed glial cell processes with lighter filaments infiltrating the choroid (Fig. 10D). The lighter filaments could possibly indicate astrocytes or Müller cells undergoing glial–mesenchymal transition (GMT). Basal laminar deposits (BLamD) were observed in 12 weeks postinjection rat eyes. Electron micrographs from the nonatrophic region of $NaIO_3$-injected eyes showed the RPE basal surface lacking deposits (Fig. 11A). In the 12 weeks postinjection rats, deposits were observed lying between RPE basal infoldings and the basement membrane within the severely atrophic area above BrM (Fig. 11B). The BLamD were discontinuous and scalloped in shape.

Distribution of Iba-1$^+$ in Retina and Choroid

In control retinas, Iba-1$^+$ microglia/macrophages were found in the GCL and inner plexiform layer (IPL) (Figs. 12A, 12B) (arrowhead). Iba1$^+$ choroidal macrophages (arrows) were also observed in the control. The density of Iba1$^+$ cells in both retina and choroid increased at 3, 8, and 12 weeks post-$NaIO_3$ injection (Figs. 12C–H). These microglia were spread throughout the retinal layers and in the subretinal space. There was a noticeable increase in Iba-1$^+$ cells in the ONL. Moreover, we noticed a time-dependent increase in the Iba1$^+$ cells at the atrophic area (data not shown) compared to the control, with many of these cells having an amoeboid morphology characteristic of activation.

Discussion

In this study, we further investigated the phenotypic characteristics of our subretinally delivered $NaIO_3$ rat model, which exhibits progressive retinal pathologic changes resembling human GA. We paid particular attention to the atrophic progression and morphologic changes of RPE, ELM descent, subretinal glial membranes, BLamD, and ORTs, which are primary features of human GA. GA is a progressive degenerative macular disease that results in loss of central vision.[6,7] Assessing the border region could yield insights into GA pathogenesis, as well as the progression of this condition.[4] In the current rat model, we observed apparent enlargement of the RPE atrophic area over time with expansion at the border. Therefore, this rat model will be useful for studying the pathologic changes associated with atrophy over time.

Zanzottera et al.[8] have demonstrated the differences in the shape of curvature of ELM descent, which delimits the atrophy in human GA. The subretinal $NaIO_3$ rat model mimicked two different types of ELM descent: oblique and curved. ELM descent at 12 weeks may represent a phase of ORT formation. ORT has been suggested to form as Müller cells attempt to protect the photoreceptors.[9] The presence of ORTs near the border region in this model is similar to those described in human GA. Therefore, this model may clarify the role Müller cells play in ORT formation and function. Similar to what has been observed in GA and other retinal degeneration studies, we also showed rhodopsin accumulation within the photoreceptor cell bodies located in the ONL adjacent to the atrophic border region.[10,11] A possible explanation for this observation is that rhodopsin synthesis persists even after the photoreceptor outer segments are lost. As the rod cells degenerate and lose their outer segments, the newly produced rhodopsin cannot be properly transported to its usual cellular location, resulting in its accumulation near the site of synthesis, specifically the photoreceptor cell soma.[12–14]

Our histology and immunofluorescence analyses demonstrated RPE disturbance near the atrophic border, including hypertrophy, and a marked reduction in expression of the RPE-65 and ZO-1. These observations suggest that breakdown of tight junctions precedes cell loss. Some RPE cells appeared to be undergoing epithelial–mesenchymal transition (EMT) as indicated by their spherical shape, multilayering, and loss of RPE-65 and ZO-1. Similar RPE structural changes have been described in human GA cases.[15–17] We have previously reported RPE migration into the retina in this model.[3] Therefore, this model could provide an experimental system for exploring the potential role of EMT at the atrophic border in GA pathology. Another significant histopathological characteristic shared by human GA and this model is the presence of subretinal gliotic membranes within and around the areas of atrophy. We recently reported these subretinal glial membranes in GA[6,18] and in this rat model.[3] Similar glial membranes have been observed in both humans and rodents with retinal degenerations.[19,20] The consequences of these membranes, however, remain unclear. On one hand, these Müller cells could create an ELM-like structure with one another, protecting the retina from inflammatory cytokines and other substances in the subretinal space. On the other hand, the ultrastructural changes in Müller cells and their migration into the subretinal space might be an indication of GMT.[21] It is crucial to understand if Müller cells undergo such a transition as this would indicate they are forming a glial scar, similar to that seen in other parts of the central nervous system. In other areas, these glial scars are believed to inhibit tissue regeneration. In GA, these cells could create a barrier, which could interfere with the efficacy of treatments administered subretinally. In particular, a subretinal gliotic membrane could impede and hamper stem cell replacement therapy by creating a structural barrier for cells to penetrate the retina and/or interact with surviving retinal cells. The idea of glial mesenchymal transition, however, is a new concept we are just beginning to investigate.

A major observation in this study is the extension of Müller cell processes through defects in BrM and into the choroidal stroma where the choriocapillaris is degenerated. Observation of intact BrM on either side of breaks suggests that Müller cells may be penetrating through weakened sights in BrM. Müller cells are known to make metalloproteinases (MMPs),

which could disrupt BrM. Although in GA eyes, we have not observed Müller cells traversing BrM, we have reported glial cells on the choroidal side of BrM.[6,18] It is possible that studies on less advanced stage eyes could reveal glial cell processes extending through breaks in BrM. As human tissue is very hard to obtain, particularly at different disease stages, the subretinal $NaIO_3$ rat model provides an ideal platform for studying glial membrane formation and its role in GA pathology.

RPE cells are acutely killed by $NaIO_3$, and consequently, the model does not recapitulate the early AMD features like drusen formation and dense sub-RPE deposits. However, at 12 weeks postinjection of $NaIO_3$, we observed BLamD, whose geographic location resembles those seen in humans with GA.[22,23] Late BLamD indicates a significant abnormality in the RPE and is consistent with observable pigment changes in clinical assessments.[24] In AMD, particularly GA, inflammation plays a crucial role in the degenerative process.[25,26] Our control showed that retinal microglia are mainly located in the GCL and IPL. However, we observed the migration of macrophages and microglia into the ONL layer at all time points in $NaIO_3$-injected rats. This migration was observed both within the atrophy and at the atrophic border. Enhanced microglial accumulation and activation in the subretinal space have been associated with degenerative changes described in many mouse models of AMD.[27,28] The continued increase in $Iba1^+$ cells at 12 weeks indicates the prolonged inflammation occurring at the border in this model, similar to that seen in GA. Further studies are required to fully investigate the inflammatory response in this model. This observation further supports the progression of atrophy in the subretinal $NaIO_3$ model and its similarities to GA at the borders where the disease expands. This inflammation could contribute to ONL thinning and loss of photoreceptors (PR) OS/IS on the nonatrophic side of the ELM descent, where RPE cells are still present. Similar PR loss beyond the RPE atrophic border has also been reported in eyes with GA.[29]

Conclusions

Despite its acute nature, the apparent expansion of atrophy in this model and the similarities between its border and that in GA make it useful for studying expansion of the atrophic lesion in this disease. The microglial and Müller cell activation and migration into the subretinal space at the border even at 12 weeks post-$NaIO_3$ injection indicate a continual inflammatory response. The translation of promising treatments from bench side to bedside relies on suitable in vivo models that are close to human pathogenesis. Provided GA's complexity, no model exists that mimics all features of the disease. In this regard, the subretinal $NaIO_3$ model has many of the pathologic changes in GA.

Acknowledgments

The authors thank Erin McDonell for assisting in preparing cryosections.

Supported by NEI/NIH R01EY031044 (ME), EY001765 (Wilmer P30 Core Grant), BrightFocus Foundation (ME), Altsheler-Durell Foundation (ME), and RPB unrestricted funds to Wilmer Eye Institute.

Disclosure: **P. Naik**, None; **R. Grebe**, None; **I.A. Bhutto**, None; **D.S. McLeod**, None; **M.M. Edwards**, None

References

1. Fleckenstein M, Mitchell P, Freund KB, et al. The progression of geographic atrophy secondary to age-related macular degeneration. *Ophthalmology*. 2018;125(3):369–390.
2. Holz FG, Strauss EC, Schmitz-Valckenberg S, van Lookeren Campagne M. Geographic atrophy: clinical features and potential therapeutic approaches. *Ophthalmology*. 2014;121(5):1079–1091.
3. Bhutto IA, Ogura S, Baldeosingh R, McLeod DS, Lutty GA, Edwards MM. An acute injury model for the phenotypic characteristics of geographic atrophy. *Invest Ophthalmol Vis Sci*. 2018;59(4):AMD143–AMD151.
4. Qu J, Velaga SB, Hariri AH, Nittala MG, Sadda S. Classification and quantitative analysis of geographic atrophy junctional zone using spectral domain optical coherence tomography. *Retina*. 2018;38(8):1456–1463.
5. Edwards MM, McLeod DS, Shen M, et al. Clinicopathologic findings in three siblings with geographic atrophy. *Invest Ophthalmol Vis Sci*. 2023;64(3):2.
6. Lindblad AS, Lloyd PC, Clemons TE, et al.; Age-Related Eye Disease Study Research Group. Change in area of geographic atrophy in the Age-Related Eye Disease Study: AREDS report number 26. *Arch Ophthalmol*. 2009;127(9):1168–1174.

7. Bird AC, Phillips RL, Hageman GS. Geographic atrophy: a histopathological assessment. *JAMA Ophthalmol*. 2014;132(3):338–345.
8. Zanzottera EC, Ach T, Huisingh C, Messinger JD, Freund KB, Curcio CA. Visualizing retinal pigment epithelium phenotypes in the transition to geographic atrophy in age-related macular degeneration. *Retina*. 2016;36(suppl 1):S12–S25.
9. Dolz-Marco R, Litts KM, Tan ACS, Freund KB,, Curcio CA. The evolution of outer retinal tubulation, a neurodegeneration and gliosis prominent in macular diseases. *Ophthalmology*. 2017;124(9):1353–1367.
10. Katschke KJ, Jr, Xi H, Cox C, et al. Classical and alternative complement activation on photoreceptor outer segments drives monocyte-dependent retinal atrophy. *Sci Rep*. 2018;8(1):7348.
11. Martinez-Navarrete G, Seiler MJ, Aramant RB, Fernandez-Sanchez L, Pinilla I, Cuenca N. Retinal degeneration in two lines of transgenic S334ter rats. *Exp Eye Res*. 2011;92(3):227–237.
12. Roof DJ, Adamian M, Hayes A. Rhodopsin accumulation at abnormal sites in retinas of mice with a human P23H rhodopsin transgene. *Invest Ophthalmol Vis Sci*. 1994;35(12):4049–4062.
13. Gao J, Cheon K, Nusinowitz S, et al. Progressive photoreceptor degeneration, outer segment dysplasia, and rhodopsin mislocalization in mice with targeted disruption of the retinitis pigmentosa-1 (Rp1) gene. *Proc Natl Acad Sci USA*. 2002;99(8):5698–5703.
14. Hollingsworth TJ, Gross AK. Defective trafficking of rhodopsin and its role in retinal degenerations. *Int Rev Cell Mol Biol*. 2012;293:1–44.
15. Curcio CA, Zanzottera EC, Ach T, Balaratnasingam C, Freund KB. Activated retinal pigment epithelium, an optical coherence tomography biomarker for progression in age-related macular degeneration. *Invest Ophthalmol Vis Sci*. 2017;58(6):BIO211–BIO226.
16. Zhang Q, Miller JML. Basic-science observations explain how outer retinal hyperreflective foci predict drusen regression and geographic atrophy in age-related macular degeneration. *Eye (Lond)*. 2022;36(5):1115–1118.
17. Guidry C, Medeiros NE, Curcio CA. Phenotypic variation of retinal pigment epithelium in age-related macular degeneration. *Invest Ophthalmol Vis Sci*. 2002;43(1):267–273.
18. Edwards MM, McLeod DS, Bhutto IA, Grebe R, Duffy M, Lutty GA. Subretinal glial membranes in eyes with geographic atrophy. *Invest Ophthalmol Vis Sci*. 2017;58(3):1352–1367.
19. Jones BW, Marc RE. Retinal remodeling during retinal degeneration. *Exp Eye Res*. 2005;81(2):123–137.
20. Wickham L, Sethi CS, Lewis GP, Fisher SK, McLeod DC, Charteris DG. Glial and neural response in short-term human retinal detachment. *Arch Ophthalmol*. 2006;124:1779–1782.
21. Kanda A, Noda K, Hirose I, Ishida S. TGF-β-SNAIL axis induces Müller glial-mesenchymal transition in the pathogenesis of idiopathic epiretinal membrane. *Sci Rep*. 2019;9(1):673.
22. Sura AA, Chen L, Messinger JD, et al. Measuring the contributions of basal laminar deposit and Bruch's membrane in age-related macular degeneration. *Invest Ophthalmol Vis Sci*. 2020;61(13):19.
23. Sarks S, Cherepanoff S, Killingsworth M, Sarks J . Relationship of basal laminar deposit and membranous debris to the clinical presentation of early age-related macular degeneration. *Invest Ophthalmol Vis Sci.* 2007;48(3):968–977.
24. Sarks JP, Sarks SH, Killingsworth MC. Evolution of geographic atrophy of the retinal pigment epithelium. *Eye (Lond)*. 1988;2(pt 5):552–577.
25. Tan W, Zou J, Yoshida S, Jiang B, Zhou Y. The role of inflammation in age-related macular degeneration. *Int J Biol Sci*. 2020;16(15):2989–3001.
26. Bakri SJ, Bektas M, Sharp D, Luo R, Sarda SP, Khan S. Geographic atrophy: mechanism of disease, pathophysiology, and role of the complement system. *J Manag Care Spec Pharm*. 2023;29(5a, suppl):S2–S11.
27. Chan CC, Ross RJ, Shen D, et al. Ccl2/Cx3cr1-deficient mice: an animal model for age-related macular degeneration. *Ophthalmic Res*. 2008;40(3–4):124–128.
28. Ufret-Vincenty RL, Aredo B, Liu X, et al. Transgenic mice expressing variants of complement factor H develop AMD-like retinal findings. *Invest Ophthalmol Vis Sci*. 2010;51(11):5878–5887.
29. Bird AC, Phillips RL, Hageman GS. Geographic atrophy: a histolopathological assessment. *JAMA Ophthalmol*. 2014;132(3):338–345.